JPE 17-6-7

https://doi.org/10.6113/JPE.2017.17.6.1454
ISSN(Print): 1598-2092 / ISSN(Online): 2093-4718

A New Dual-Active Soft-Switching Converter for an MTEM Electromagnetic Transmitter

Xuhong Wang†, Yiming Zhang*, and Wei Liu*

†,*Faculty of Information Technology, Beijing University of Technology, Beijing, China

Abstract

In this study, a new dual-active soft-switching converter is proposed to improve conversion efficiency and extend the load range for an MTEM electromagnetic transmitter in geological exploration. Unlike a conventional DC/DC converter, the proposed converter can operate in passive soft-switching, single-active soft-switching, or dual-active soft-switching modes depending on the change in load power. The main switches and lagging auxiliary switches of the converter can attain soft-switching over the entire load range. The conduction and switching losses are greatly reduced compared with those of ordinary converters under the action of the cut-off diodes and auxiliary windings coupled to the main transformer in the auxiliary circuits. The conversion efficiency of the proposed converter is significantly improved, especially under light-load conditions. First, the working principle of the proposed converter is analyzed in detail. Second, the relationship between the different operating modes and the load power is given and the design principle of the auxiliary circuit is presented. Finally, the Saber simulation and experimental results verify the feasibility and validity of the converter and a 50 kW prototype is implemented.

Key words: Auxiliary windings, Cut-off diodes, Dual-active soft-switching, MTEM transmitter

I. INTRODUCTION

After years of exploration and mining, shallow mineral resources have been substantially reduced and the main prospecting aspects are deep mines and buried ore. In electromagnetic exploration, the power of the electromagnetic wave will exponentially decay with the increase in frequency. Given the increase in depth, the resolution ratio of the detection is reduced rapidly [1]. Therefore, the key to detecting a deep mine is to greatly improve the electromagnetic field strength and increase the transmitter output power. Meanwhile, the volume and weight of the transmitter cannot be excessive in facilitating the transportation of the exploration equipment. That is, improving the power density of the transmitter is necessary.

The multi-channel transient electromagnetic method (MTEM) is a time-domain, artificial source electromagnetic method that is based on the principle of electromagnetic induction [2]. A typical geological survey is shown in Fig. 1. The MTEM transmitter injects the encoded current into the earth with different frequencies through the emitter electrodes. Given that the response of electromagnetic waves by different ore bodies is not the same, the receivers detect the signal differences and then attain detection of the ore bodies [3].

The earth is the load of the MTEM transmitter; the load characteristics vary with the output frequency, and the load impedance changes from several ohms to hundreds of ohms continuously. The curves of the load impedance and the output frequency are shown in Fig. 2. The stable output characteristics of the MTEM transmitter are required over the entire load range [3], [4].

Several transmitters have been developed to date. An American company, Zonge International, has developed the GGT-30 transmitter with an output power of 30 kW. The Canadian Phoenix TXU-30 transmitter achieves an output power of 20 kW [5]. Current transmitters present many problems, such as low power density, low output efficiency, and narrow dynamic range. These properties cannot meet the actual needs of geological explorations.

The core part of the transmitter is a DC/DC controllable source circuit that determines the overall performance of the transmitter. The soft-switching controlled-source technology can solve the above-mentioned problems. Many topologies

Manuscript received Apr. 24, 2017; accepted Aug. 4, 2017
Recommended for publication by Associate Editor Chun-An Cheng.
†Corresponding Author: wangxuhong0909@163.com
Tel: +86-10-6739-6621, Fax: +86-10-6739-6621, Beijing Univ. of Tech.
*Faculty of Information Tech., Beijing University of Technology, China

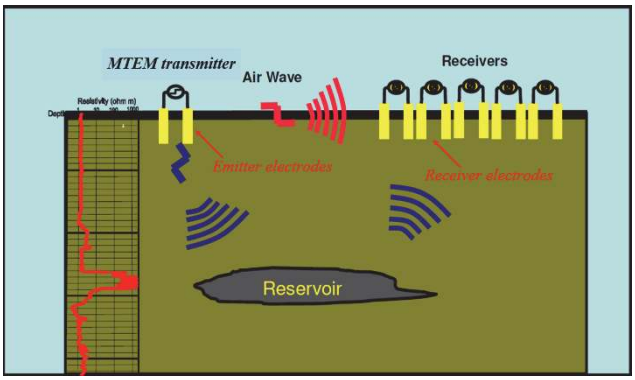

Fig. 1. Technique of MTEM geological exploration.

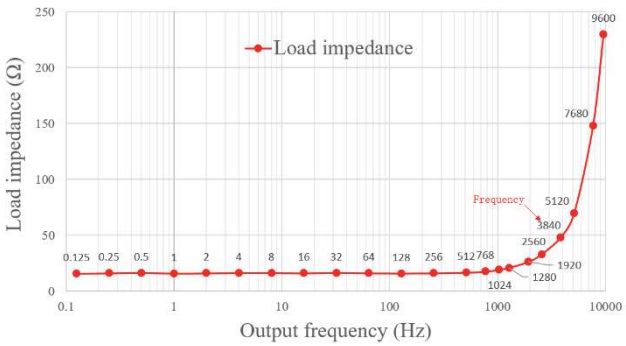

Fig. 2. Curves of the load impedance and output frequency.

exist for the soft-switching controlled-source circuit and apply different power levels [6]-[9]. Given that the transmitter must output high voltage and high power, a phase-shifted full-bridge (PSFB) DC/DC converter is adopted for the transmitter. A PSFB converter is widely used in medium- and high-power applications. The main switches of the PSFB converter can achieve zero-voltage-switching (ZVS) with the energy stored in the saturated reactor, the resonant inductor, and the transformer leakage inductance [9]-[14]. The voltage and current stress and the switching losses are greatly reduced because of the application of the passive soft-switching technology [12]-[14]. However, the passive soft-switching converter is limited by its narrow output dynamic range. Therefore, increasing the resonant inductance is necessary to extend the converter's operating range. Large resonant inductance means significant loss of the duty cycle. Producing voltage ringing across the high-frequency rectifiers of the transformer's secondary side is easy [15]. A saturated reactor was used in [16] to reduce the loss of the duty cycle of the secondary side. However, this reactor does not apply to a high-power output. In the case of high-power output, the saturated reactor will seriously overheat, which will increase not only the loss but also the risk to the system. In the case of a light load, achieving ZVS in the lagging leg of the passive soft-switching converter is difficult owing to the insufficient energy stored in the resonant inductor. This condition will not only result in a low-output efficiency and serious electromagnetic interference but also easily lead to insulated gate bipolar transistor (IGBT) burn-down under high voltage and current stress conditions. Therefore, an auxiliary current source network was introduced in [17] to solve the failure of the lagging leg switches in realizing ZVS under a light load. The auxiliary current source together with the primary current of the high-frequency transformer is used for charging and discharging the resonant capacitors in parallel with the main arm switches to ensure ZVS at low power levels [18]. An auxiliary current source network contains a variety of structures [19]-[21] that extend the load-operating range to a certain extent. However, the circuit loss increases as a result of the circulating loss in the transformer's primary side and the loss of the added auxiliary circuits. The topology in [22] solves the problem of the loop current loss, but the lack of the main resonant inductor leads to the failure of the main switches' ZVS for high-output power. In addition, these topologies ignore the ZVS of the leading leg and are thus limited. In geological exploration, the load is not constant as it varies with the output frequency. When the energy stored in the transformer leakage inductance and the output filter inductor is too small to ensure ZVS of the leading leg, the voltage of the resonant capacitor will experience a severe shock and the capacitor will seriously overheat or even burn out [23], [24], thereby causing security risks to the system. Although the active auxiliary circuits reported in [25] and [26] can help the leading leg to achieve ZVS, these circuits cannot guarantee ZVS under a full load range and increase the conduction loss.

In this study, a novel dual-active soft-switching circuit is proposed to guarantee the ZVS of the main switches for the entire range of the load. The leading auxiliary leg achieves ZVS, whereas the lagging auxiliary leg achieves zero-current-switching (ZCS). In practical application, the proposed converter can operate in passive soft-switching, single-active soft-switching, and dual-active soft-switching modes depending on the change in the load power in improving the efficiency. When all the main switches can realize ZVS with the energy stored in the resonant inductor, the converter operates in passive soft-switching mode. At light load level, the lagging switches cannot achieve ZVS, but the leading switches can realize ZVS. Therefore, the proposed converter works in single-active soft-switching mode. When the output power continues to decrease and the leading switches cannot realize ZVS, the converter operates in dual-active soft-switching mode. This method greatly broadens the operating range of the converter and ensures the safety and stability of the system. Only when the upper or lower tubes are on the same leg switch will current flow in the auxiliary circuit. Thus, the RMS value of the auxiliary loop current is greatly reduced and the efficiency of the converter is improved.

The rest of the paper is organized as follows. The topology of the dual-active soft-switching converter and the timing

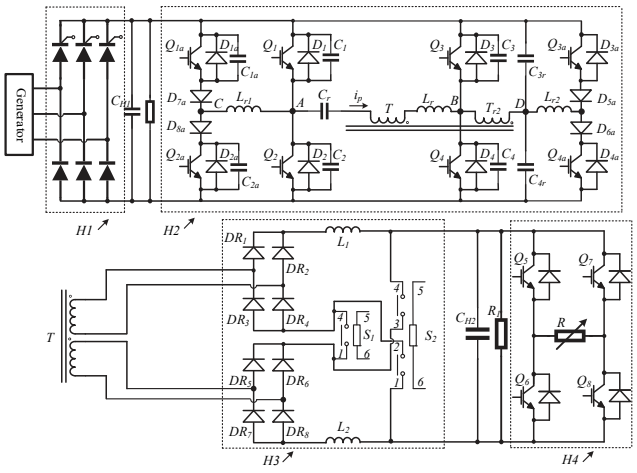

Fig. 3. Topology of MTEM electromagnetic transmitter.

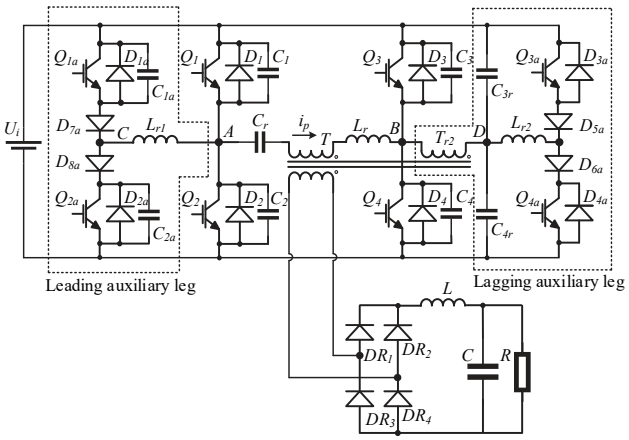

Fig. 4. Topology of the dual-active soft-switching converter.

diagram of the control signal are described in Section II. The working principle of the proposed converter is analyzed in detail in Section III. The switching conditions of the proposed converter among passive, single-active, and dual-active soft-switching modes as well as the design principles of the auxiliary circuit are described in Section IV. The Saber simulation and experimental results of a 50 kW prototype are discussed in Section V. The conclusion and references are presented in Section VI.

II. Dual-Active Soft-Switching Converter

The topology of the MTEM electromagnetic transmitter is shown in Fig. 3. The transmitter system mainly includes four parts: a three-phase half-controlled rectifier filter circuit *H1*, a low-voltage inverter bridge *H2*, a high-frequency rectifier bridge *H3*, and a high-voltage inverter bridge *H4*.

The line voltage of the three-phase generator is 380 V and the frequency is 50 Hz. The function of the three-phase half-controlled rectifier filter circuits *H1* is to convert the alternating current into low-voltage direct current. Next, the current is converted to high-voltage DC by the inverter bridge *H2* and the rectifier bridge *H3*. Finally, the current can be converted to high-voltage AC with a different frequency through the inverter bridge *H4*. These high-voltage signals are injected into the earth through the emission electrodes.

As shown in Fig. 3, if the series relay (S_1) is selected, then the two rectifier bridges are connected in series. The maximum voltage of the MTEM transmitter can reach 1000 V and the maximum current can be up to 50 A. If the parallel relay (S_2) is selected, then the two rectifier bridges are connected in parallel. The maximum output voltage of the transmitter is 500 V, and the maximum output current can reach 100 A. In geological exploration, the load impedance is related not only to the output frequency but also to the geological structure. In the desert area, the transmitter needs to significantly increase the output voltage to increase the output current. The series structure (S_1 is selected) should be adopted. The impedance is small of the swamp area, and the output current can be greater than 50 A although the output voltage is very low. The parallel structure (S_2 is selected) should be adopted. In most cases, the low-frequency load impedance is greater than 10 Ω and the transmitter adopts the series structure. Only when the low-frequency load impedance is less than 10 Ω will the transmitter adopt the parallel structure. The transmitter can adapt to a wide range of geological conditions, such as desert or marsh environment, with the structure of H_2 and H_3. The proposed prototype transmitter adopts the series structure.

The analysis above shows that the DC/DC converter is the core part of the MTEM electromagnetic transmitter and its stability and efficiency directly affect the performance of the transmitter. The dual output circuits of the high-frequency transformer are simplified to a single output and the inverter bridge *H4* is removed and replaced with a variable resistor to facilitate the analysis. Therefore, Fig. 3 is simplified as shown in Fig. 4.

The topology of the dual-active soft-switching converter is shown in Fig 4. The leading leg is formed by the switches Q_1 and Q_2, and the lagging leg is composed of the switches Q_3 and Q_4. The blocking capacitor C_r is used to filter out the DC component in the high-frequency transformer to prevent the magnetic deflection of the transformer. The resonant capacitors C_1, C_2, C_3, and C_4 connected in parallel to the main switches are resonated with the resonant inductor L_r to ensure that the main switches can achieve ZVS. The high-frequency rectifier bridge is composed of the diodes DR_1, DR_2, DR_3, and DR_4. The inductor L and the capacitor C constitute a low-pass filter circuit to ensure output voltage and current stability.

As shown in Fig. 4, the lagging auxiliary leg is formed by the devices Q_{3a}, Q_{4a}, C_{3r}, C_{4r}, D_{5a}, D_{6a}, L_{r2}, and the auxiliary winding T_{r2}. When the output load current is less than a certain value, the lagging auxiliary leg turns on to ensure that the lagging leg realizes ZVS. The devices Q_{1a}, Q_{2a}, C_{1a}, C_{2a}, D_{7a}, D_{8a}, and the inductor L_{r1} form the leading auxiliary leg. When

the output load current continues to decrease, the leading auxiliary leg turns on to ensure that the leading leg realizes ZVS.

The main waveforms of the proposed converter under different operating modes are shown in Fig. 5. V_{g1}, V_{g2}, V_{g3}, and V_{g4} are the driving signal waveforms of the main switches in the phase-shifted control mode. V_{g1a} and V_{g2a} are the driving signals of the leading auxiliary leg. The leading auxiliary switches Q_{2a} and Q_{1a} are turned on before the main switches Q_1 and Q_2 are turned off to store energy in the resonant inductor L_{r1}. Q_{2a} and Q_{1a} are turned off after the main switches Q_2 and Q_1 are turned on. Similarly, V_{g3a} and V_{g4a} are the driving signals of the lagging auxiliary leg. The lagging auxiliary switches Q_{3a} and Q_{4a} are turned on before the main switches Q_4 and Q_3 are turned off to store energy in the resonant inductor L_{r2}. Q_{3a} and Q_{4a} are turned off after the main switches Q_3 and Q_4 are turned on.

As shown in Fig. 4, the auxiliary winding T_{r2} provides a back electromotive force in the lagging auxiliary circuits to ensure that the lagging auxiliary switches attain ZCS. Owing to the effect of the cut-off diodes D_{5a}, D_{6a}, D_{7a}, and D_{8a}, the current flows through the auxiliary circuit during the opening of the auxiliary switches; otherwise, the current is zero. According to the information in literature [19], the conduction loss of the auxiliary circuit and the lagging leg should be greatly reduced. Given that the RMS value of the current flowing in the auxiliary winding T_{r2} is greatly reduced, the introduction of the auxiliary winding does not cause a significant increase in the core volume of the main transformer.

III. Operational Principle of the Dual-Active Soft-Switching Converter

The operational process of the proposed converter is analyzed in detail in this section. When the leading and lagging auxiliary circuits are turned on and work together with the main switches on the basis of the timing waveforms shown in Fig. 5, the proposed converter possesses 18 operating modes in a working cycle. In practical applications, the two auxiliary circuits are selectively turned on or off depending on the change in the load power. This condition will not affect the principle analysis of the converter. We propose the following assumptions to simplify the analysis process:

1. All IGBTs, diodes, inductors, capacitors, and transformers in the converter are ideal components.

2. The parallel resonant capacitors of the main switches: $C_1=C_2=C_{lead}$, $C_3=C_4=C_{lag}$.

3. The resonant capacitors of the auxiliary switches: $C_{1a}=C_{2a}=C_{aux1}$, $C_{3r}=C_{4r}=C_{aux2}$.

4. $L>>L_r/K^2$, where L is the output filter inductor and K represents the turns ratio of the primary and secondary windings of the transformer.

5. Q_1 and Q_2 are the leading switches while Q_3 and Q_4 are the lagging switches. Q_{1a} and Q_{2a} are the leading auxiliary switches while Q_{3a} and Q_{4a} are the lagging auxiliary switches.

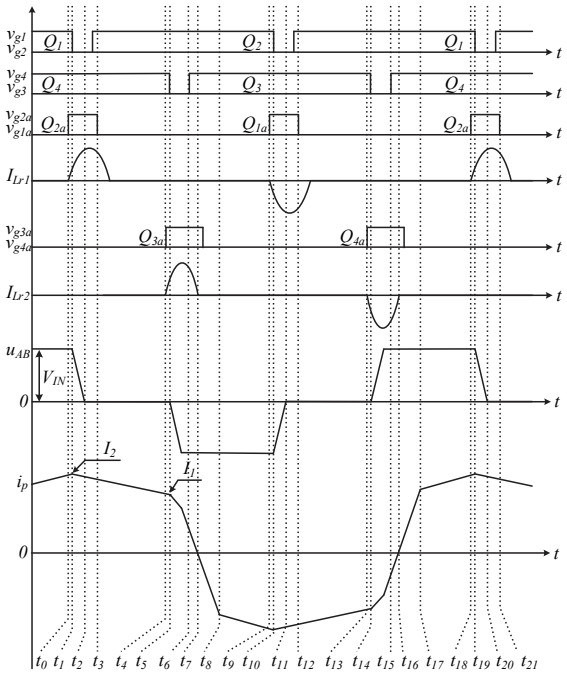

Fig. 5. Key waveforms of the dual-active soft-switching converter.

Mode 1 ($0<t<t_0$): As shown in Fig. 6(a), the main switches Q_1 and Q_4 and the high-frequency rectifier diodes DR_2 and DR_3 are in conduction, thereby carrying the energy to the load. The current that flows through the primary winding of the transformer is i_p. At t_0, the leading auxiliary switch Q_{2a} is turned on to charge the inductor L_{r1} and ensure that the leading switch Q_2 realizes ZVS.

Mode 2 ($t_0<t<t_1$): In this period, the devices Q_1, Q_4, DR_2, and DR_3 remain in conduction, thereby carrying the energy to the load. The leading auxiliary switch Q_{2a} is turned on at t_0, and the current flows through the devices Q_1, L_{r1}, D_{8a}, and Q_{2a} to charge the inductor L_{r1} as shown in Fig. 6(b). At the end of this mode, the leading switch Q_1 is turned off.

Mode 3 ($t_1<t<t_2$): At t_1, the leading switch Q_1 is turned off. The transformer primary current i_p and the inductor current i_{Lr1} charge the resonant capacitor C_1 and discharge the capacitor C_2 simultaneously. The leading switch Q_1 achieves zero-voltage turn-off because of the effect of the capacitor C_1. The voltage of the capacitor C_2 and u_{AB} are zero at t_2. Thus, the diode D_2 is naturally in conduction. In the period of time t_1–t_2, the resonant inductor L_r and the output filter inductor L are equivalent series. The equations of the primary current i_p and the capacitor voltage v_{C1}, v_{C2} are as follows:

$$i_p(t) = I_P(t_1) = I_2\,, \tag{1}$$

$$v_{C_1}(t) = \frac{I_2}{2C_{lead}}(t - t_1)\,, \tag{2}$$

$$v_{C_2}(t) = V_{IN} - \frac{I_2}{2C_{lead}}(t - t_1)\,. \tag{3}$$

Mode 4 ($t_2<t<t_3$): As shown in Fig. 6(d), no current is

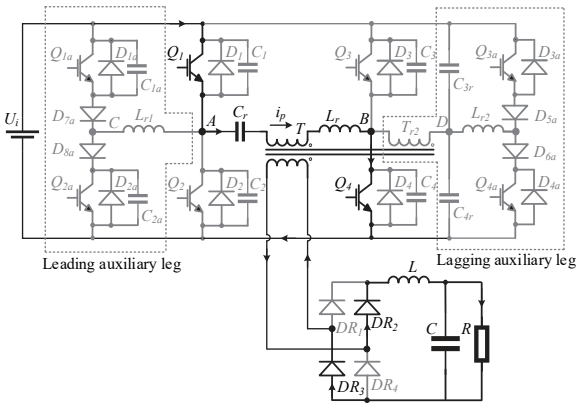

(a) Mode 1: 0–t_0.

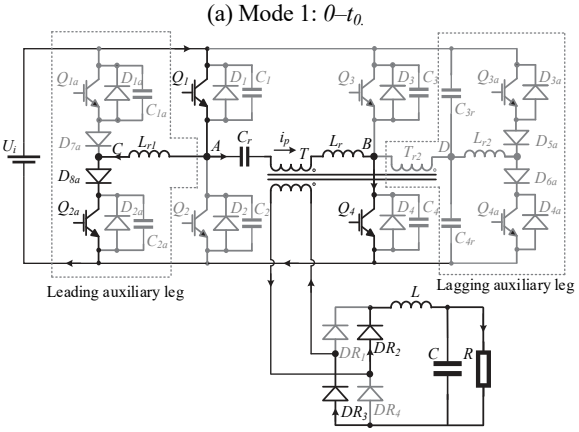

(b) Mode 2: t_0–t_1.

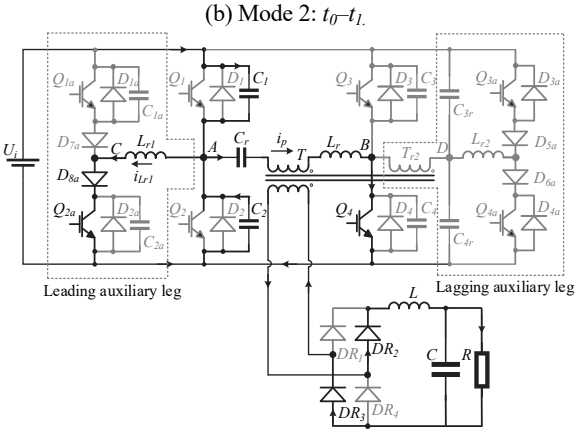

(c) Mode 3: t_1–t_2.

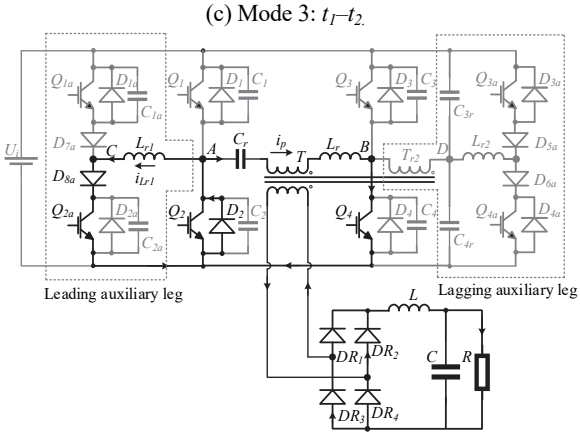

(d) Mode 4: t_2–t_3.

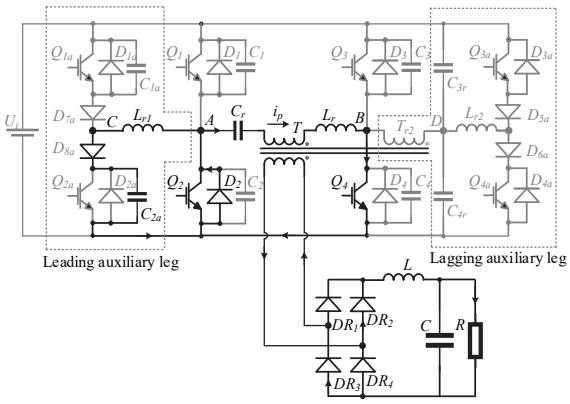

(e) Mode 5: t_3–t_4.

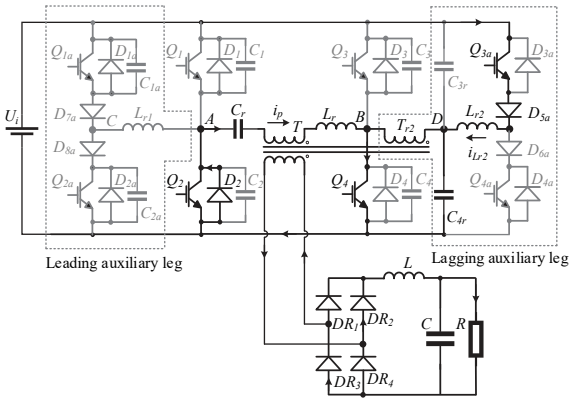

(f) Mode 6: t_4–t_5.

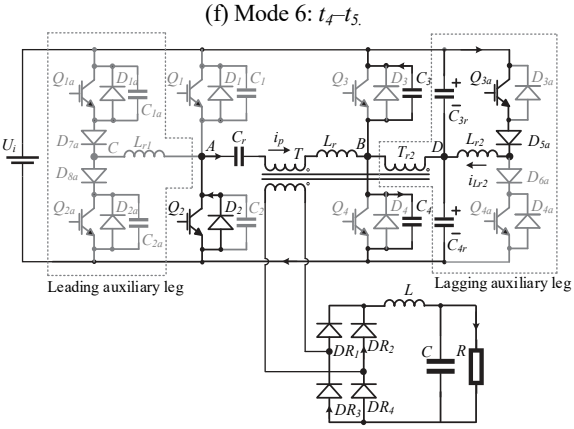

(g) Mode 7: t_5–t_6.

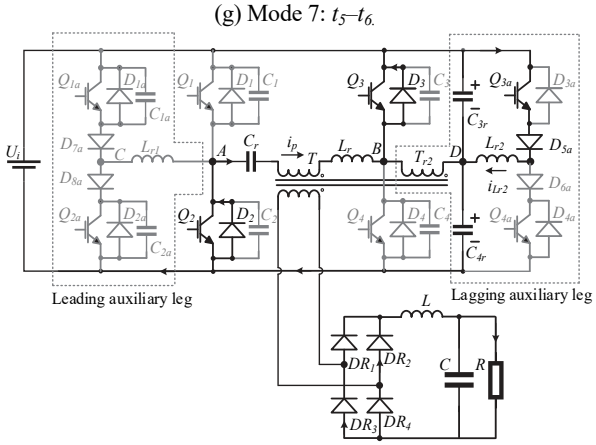

(h) Mode 8: t_6–t_7.

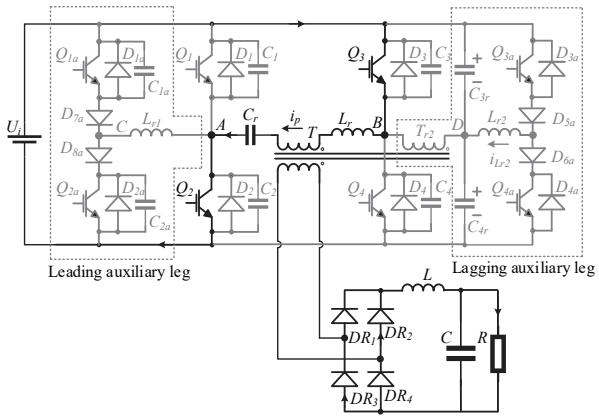

(i) Mode 9: t_7–t_8.

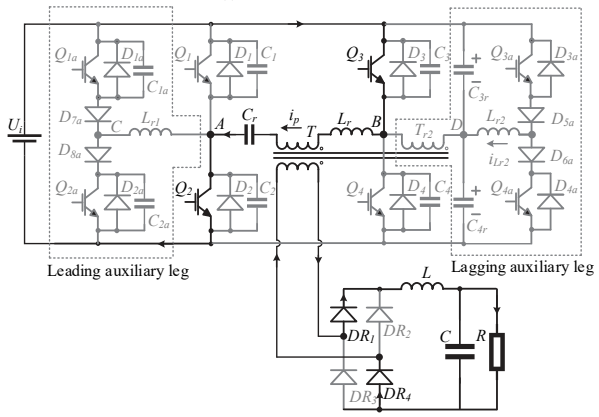

(j) Mode 10: t_8–t_9.

Fig. 6. Operation of the dual-active soft-switching converter.

flowing in the switch Q_2 although Q_2 is turned on. The current flows through the diode D_2 to ensure that Q_2 realizes zero-voltage turn-on. The dead time of the driving signals in the leading leg needs to conform to the following equation:

$$T_{d(lead)} > \frac{2C_{lead} \cdot V_{IN}}{I_2}. \tag{4}$$

Mode 5 (t_3<t<t_4): The auxiliary switch Q_{2a} achieves the zero-voltage turn-off at t_3. During t_3–t_4, the voltage u_{AB} is zero and the diode D_2 remains in the freewheeling state and the transformer's primary current i_p is equal to the reflected filter inductor current.

$$i_p(t) = i_{L(t)} / K \tag{5}$$

The lagging auxiliary switch Q_{3a} is opened at t_4 before the lagging switch Q_4 is turned off.

Mode 6 (t_4<t<t_5): The auxiliary switch Q_{3a} achieves zero-current turn-on at t_4. In mode 6, the current flows through the devices Q_{3a}, D_{5a}, L_{r2}, T_{r2}, and Q_4 to charge the inductor L_{r2} as shown in Fig. 6(f) and the voltage u_{AB} remains zero. At t_5, the lagging switch Q_4 attains zero-voltage turn-off.

In this interval, the proposed converter remains in a freewheeling state and all the diodes of the output rectifier are in conduction. Owing to the clamping of the transformer's secondary windings, the voltage across the primary windings of the transformer is also zero. In this freewheeling interval, v_{C2} = v_{C4} = 0, v_{C1} = v_{C3} = V_{IN}, v_{C4r} = 0, v_{C3r} = V_{IN}. At t = t_4, the auxiliary switch Q_{3a} is gated. The voltage across the resonant inductor (L_{r2}) is V_{IN}. The current in the lagging auxiliary inductor L_{r2} can be expressed as follows:

$$i_{L_{r2}}(t) = \frac{V_{IN}}{L_{r2}}(t - t_4). \tag{6}$$

Mode 7 (t_5<t<t_6): At t_5, the lagging switch Q_4 is turned off. The transformer's primary current i_p and the inductor current i_{Lr2} charge the resonant capacitor C_4 and discharge the capacitor C_3 simultaneously. The voltage of the capacitor C_3 is reduced to zero and the diode D_3 is turned on.

The equations of the primary current i_p and the capacitor voltage v_{C3}, v_{C4} during this mode are as follows:

$$i_p(t) = (I_1 + I_{Lr2})\cos w_1(t - t_5) - I_{Lr2}, \tag{7}$$

$$v_{C_4}(t) = (I_1 + I_{Lr2})Z_1 \sin w_1(t - t_5), \tag{8}$$

$$v_{C_3}(t) = V_{IN} - (I_1 + I_{Lr2})Z_1 \sin w_1(t - t_5), \tag{9}$$

where $Z_1 = \sqrt{L_r / (2C_{lag})}$, $w_1 = 1/\sqrt{2L_rC_{lag}}$.

The voltage of the resonant capacitor C_{3r} can be expressed as follows:

$$v_{C_{3r}}(t) = V_{IN} \cos w(t - t_5), \tag{10}$$

where $w = 1/\sqrt{L_{r2}C_{3r}}$.

At t_6, the voltage of the resonant capacitor C_{3r} and C_{4r} can be expressed as follows:

$$v_{C_{3r}}(t_6) = -\frac{V_{IN}}{n_{aux}}, \tag{11}$$

$$v_{C_{4r}}(t_6) = V_{IN}\left(\frac{n_{aux} + 1}{n_{aux}}\right), \tag{12}$$

where n_{aux} is the turns ratio of the primary windings and the auxiliary windings (T_{r2}).

In accordance with Eqs. (10) and (11), t_5 to t_6 can be obtained as follows:

$$T_{falling} = t_6 - t_5 = \frac{1}{w}\arccos\left(\frac{-1}{n_{aux}}\right). \tag{13}$$

Mode 8 (t_6<t<t_7): As shown in Fig. 6(h), no current is flowing in the lagging switch Q_3 although Q_3 is turned on because the primary current i_p and the inductor current i_{Lr2} flow through the diode D_3 to ensure Q_3 realizes zero-voltage turn-on. According to the dotted terminals of the primary and auxiliary windings, the auxiliary windings T_{r2} provides an electromotive force that is opposite to the direction of the current i_{Lr2} such that the inductor current i_{Lr2} is gradually reduced. At t_7, the current i_{Lr2} is reduced to zero but the lagging auxiliary switch Q_{3a} is not turned off. The dead time $T_{d(lag)}$ between the main switches Q_3 and Q_4 should be greater than t_{67} and can be expressed as Eq. (14).

$$T_{d(lag)} > \frac{1}{w_1}\arcsin\frac{V_{IN}}{Z_1 I_1} \tag{14}$$

The primary current of the transformer can be expressed as follows:

$$i_p(t) = I_p(t_6) - \frac{V_{IN}}{L_r}(t - t_6). \quad (15)$$

Mode 9 (t_7<t<t_8): As shown in Fig. 6(i), the primary current i_p drops to the zero-crossing at t_7 and the switches Q_3 and Q_2 provide access for the current i_p. Given that the current i_p is insufficient to provide energy for the load, the four diodes of the high-frequency rectifier bridge are all in conduction. Therefore, the primary voltage of the transformer is zero. At the end of this mode, the diodes DR_2 and DR_3 are turned off. The current i_p can be expressed as Eq. (16).

$$i_p(t) = -\frac{V_{IN}}{L_r}(t - t_7) \quad (16)$$

Mode 10 (t_8<t<t_9): In mode 10, the main switches Q_2 and Q_3 and the high-frequency rectifier diodes DR_1 and DR_4 are in conduction, thereby carrying the energy to the load. The primary current i_p is the reverse of that in mode 1.

During this period, the current i_p can be expressed as follows:

$$i_p(t) = -\frac{V_{IN} - KV_{out}}{L_r + K^2 L}(t - t_8). \quad (17)$$

To ensure that Q_1 achieves ZVS under a light load, the leading auxiliary switch Q_{1a} is opened at t_9 to charge the inductor L_{r1} before the leading switch Q_2 is turned off. The work of the other half cycle of the proposed converter is similar to that of the above-mentioned half cycle.

IV. Design and Implementation of the Proposed Converter

Duty cycle loss on the secondary side of the transformer is a unique phenomenon for the ZVS phase-shift full-bridge converter. As shown in Figs. 5 and 6(g), (h), and (i), the time that the primary current i_p varies from positive to negative is t_5 to t_8. In this period, the primary voltage u_{AB} is established but the primary current is insufficient to provide the load current. The rectifier diodes of the secondary side are all in the freewheeling state; the secondary voltage of the transformer is zero during t_5–t_8. Therefore, the duty cycle loss of the transformer's secondary side can be expressed as follows:

$$D_{loss} = \frac{t_{58}}{T_s/2} \approx \frac{L_r[I_1 + I_L(t_5)/K]}{V_{IN}}, \quad (18)$$

where t_{58} represents t_5–t_8.

Assuming that the load current exhibits small fluctuations at t_5, $I_L(t_5)$=I_{out}, then Eq. (18) can be expressed as Eq. (19).

$$D_{loss} \approx \frac{4L_r I_{out}}{KT_s V_{IN}} \quad (19)$$

According to Eq. (19), large resonant inductance L_r means significant loss of the secondary duty cycle. Therefore, to ensure that the main switches achieve ZVS and the efficiency of the converter, the resonant inductance cannot be too large.

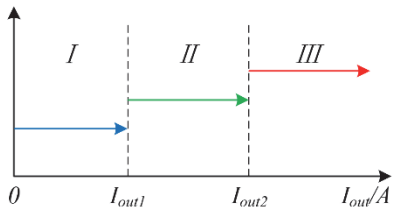

Fig. 7. Relationship between the operating mode and the load current.

Assuming that the load current is reduced to the minimum I_{out2}, then the energy stored in the resonant inductor L_r can still ensure that the main switches achieve ZVS. If the load current continues to decrease until the lagging switches cannot realize ZVS, then the lagging auxiliary leg of the proposed converter is opened. When the load current is further reduced to I_{out1} and the leading switches cannot achieve ZVS, the leading auxiliary leg of the proposed converter is opened.

Therefore, the proposed converter can realize ZVS for a wider range than does the traditional converter.

The relationship between the operating mode of the proposed converter and the load current is shown in Fig. 7.

I: For dual-active soft-switching, the leading and lagging auxiliary legs are opened.

II: For single-active soft-switching, only the lagging auxiliary leg is opened.

III: For passive soft-switching, the leading and lagging auxiliary legs are closed.

A. ZVS Conditions of the Leading Leg and Lagging Leg

The analysis of the operating process of the proposed converter shown in Fig. 6 indicates that the energy should be sufficient to fully charge and discharge the resonant capacitors in parallel with the main switches in the same leg. Considering the influence of the parasitic capacitance on the primary windings of the high-frequency transformer, part of the energy is required to provide the parasitic capacitance C_{tr}.

Therefore, to ensure that the main switches realize ZVS, the energy for the leading leg needs to meet the conditions in the following equation:

$$\begin{aligned} E &> \frac{1}{2}C_{lead}V_{IN}^2 + \frac{1}{2}C_{lead}V_{IN}^2 + \frac{1}{2}C_{TR}V_{IN}^2 \\ &= C_{lead}V_{IN}^2 + \frac{1}{2}C_{TR}V_{IN}^2 \end{aligned}. \quad (20)$$

The energy for the lagging leg needs to meet the conditions in Eq. (21).

$$\begin{aligned} E &> \frac{1}{2}C_{lag}V_{IN}^2 + \frac{1}{2}C_{lag}V_{IN}^2 + \frac{1}{2}C_{TR}V_{IN}^2 \\ &= C_{lag}V_{IN}^2 + \frac{1}{2}C_{TR}V_{IN}^2 \end{aligned} \quad (21)$$

The analysis of mode 3 indicates that the energy for the resonant capacitors of the leading leg is provided by the resonant inductor L_r and the filter inductor L. Therefore, the leading leg can easily achieve ZVS.

However, the analysis of mode 7 shows that the energy for the resonant capacitors of the lagging leg is only supplied by the resonant inductor L_r. Therefore, achieving ZVS for the lagging leg is more difficult than for the leading leg.

B. Switching Conditions for the Lagging Auxiliary Leg

In accordance with the analysis of mode 6, the relationship between the primary current i_p and the filter inductor current can be obtained as Eq. (22).

$$i_p(t) = i_L(t)/K \tag{22}$$

The primary current i_p is reduced to I_1 as shown in Fig. 5. The latter is expressed as Eq. (23).

$$I_1 = i_L(t_5)/K = I_L / \mathrm{K} \tag{23}$$

Assuming that the current in the inductor L_{r2} is I_a, then Eqs. (7)–(9) can be expressed as follows:

$$i_p(t) = (I_1 + I_a)\cos w_1(t - t_5) - I_a , \tag{24}$$

$$v_{C_4}(t) = (I_1 + I_a)Z_1 \sin w_1(t - t_5) , \tag{25}$$

$$v_{C_3}(t) = V_{IN} - (I_1 + I_a)Z_1 \sin w_1(t - t_5) . \tag{26}$$

According to Eqs. (24) and (25), when the resonant capacitor voltage rises to V_{IN}, the primary current does not drop to $-I_1$, or the primary current drops to $-I_1$, the auxiliary current I_a provides the remaining energy. Therefore, at the end of mode 7, i_p and I_a need to meet the conditions in the following equations:

$$i_p(t) = (I_1 + I_a)\cos w_1(t - t_5) - I_a \geq -I_1 , \tag{27}$$

$$i_a(t) \geq 0 . \tag{28}$$

In accordance with Eq. (27), the time $t_5^{'}$ when the primary current drops to $-I_1$ can be expressed as

$$t_5^{'} = t_5 + \frac{1}{w_1}\arccos\left(\frac{I_a - I_1}{I_a + I_1}\right) . \tag{29}$$

The voltage of the resonant capacitor C_4 can be obtained as follows:

$$\begin{aligned} v_{C_4}(t_5^{'}) &= (I_1 + I_a)Z_1 \sin w_1(t_5^{'} - t_5) \\ &= (I_1 + I_a)Z_1 \sin\left[\arccos\left(\frac{I_a - I_1}{I_a + I_1}\right)\right] . \end{aligned} \tag{30}$$

If $t_5^{'}$ is taken as the demarcation point, then the current i_p and the voltage v_{C4} can be expressed as

$$\begin{cases} i_p(t) = (I_1 + I_a)\cos w_1(t - t_5) - I_a \\ v_{C_4}(t) = (I_1 + I_a)Z_1 \sin w_1(t - t_5) \end{cases} \quad t \in [t_5, t_5^{'}] \tag{31}$$

$$\begin{cases} i_p(t) = -I_1 \\ v_{C_4}(t) = v_{C_4}(t_5^{'}) + \dfrac{I_a - I_1}{2C_{lag}}(t - t_5^{'}) \end{cases} \quad t \in [t_5^{'}, t_6] \tag{32}$$

According to Eq. (32), if the current i_p is not reduced to $-I_1$ and the voltage v_{C4} is increased to V_{IN}, then v_{C4} needs to meet the conditions in the following equation to ensure ZVS of the lagging switches:

$$v_{C_4}(t) = (I_1 + I_a)Z_1 \sin w_1(t - t_5) \geq V_{IN} . \tag{33}$$

According to Eq. (19), the value of $(I_1 + I_a)Z_1$ should be as small as possible to reduce the secondary duty cycle loss. Therefore, the value of $\sin w_1(t - t_5)$ is appropriate when between 0.9 and 1. Then, Eq. (33) can be expressed as Eq. (34).

$$(I_1 + I_a)Z_1 \geq V_{IN} \tag{34}$$

Therefore, the relationship between the lagging auxiliary current I_a and the load current I_L can be derived as Eq. (35).

$$I_a = \frac{V_{IN}}{Z_1} - \frac{I_L}{K} \tag{35}$$

If I_a=0, then

$$I_L = \frac{KV_{IN}}{Z_1} . \tag{36}$$

According to Eq. (32), if the primary current i_p is reduced to $-I_1$ and the voltage v_{C4} is not increased to V_{IN}, then v_{C4} needs to meet the conditions in Eq. (37) to ensure ZVS of the lagging switches.

$$v_{C_4}(t) = v_{C_4}(t_5^{'}) + \frac{I_a - I_1}{2C_{lag}}(t - t_5^{'}) \geq V_{IN} \tag{37}$$

Equation (37) is a nonlinear equation and obtaining its analytical solution is difficult. In accordance with Eq. (30) and Fig. 5, Eq. (37) can be derived as Eq. (38).

$$\frac{I_a - I_1}{2C_{lag}} t_{d(lag)} \geq V_{IN} , \tag{38}$$

where $t_{d(lag)}$ is the dead time of the driving signal for the lagging leg.

The relationship between I_a and I_L can be expressed as follows:

$$I_a = \frac{2V_{IN}C_{lag}}{t_{d(lag)}} + \frac{I_L}{K} . \tag{39}$$

In accordance with Eqs. (35) and (39), the maximum value of the lagging auxiliary current $I_{a(max)}$ can be derived as follows:

$$I_{a(\max)} = V_{IN}\left(\frac{1}{2Z_1} + \frac{C_{lag}}{t_{d(lag)}}\right) \tag{40}$$

The relationship between I_a and I_L can be expressed as Eq. (41).

$$I_a = \begin{cases} \dfrac{2V_{IN}C_{lag}}{t_{d(lag)}} + \dfrac{I_L}{K} & 0 < I_L \leq K \cdot V_{IN}\left(\dfrac{1}{2Z_1} - \dfrac{C_{lag}}{t_{d(lag)}}\right) \\ \dfrac{V_{IN}}{Z_1} - \dfrac{I_L}{K} & K \cdot V_{IN}\left(\dfrac{1}{2Z_1} - \dfrac{C_{lag}}{t_{d(lag)}}\right) < I_L \leq \dfrac{KV_{IN}}{Z_1} \\ 0 & I_L > \dfrac{KV_{IN}}{Z_1} \end{cases} \tag{41}$$

In accordance with Eq. (41), Fig. 8 provides the relationship between the lagging auxiliary current (i_a) and the load current (i_L).

C. Switching Condition for the Leading Auxiliary Leg

As shown in Figs. 5 and 6(b), the primary current is I_2 at

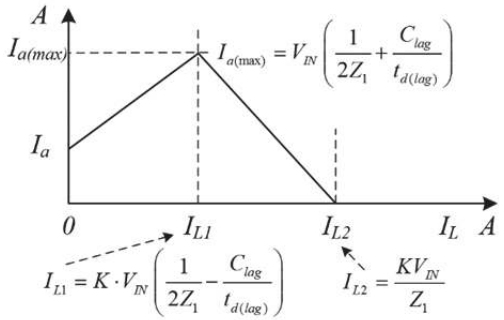

Fig. 8. Curves of i_a and i_L.

the end of mode 2. The relationship between the inductor L_r and the filter inductor L is equivalent series through the analysis of mode 3. Therefore, the primary current contains the reflected filter inductor current. It is expressed as Eq. (42).

$$I_2 = I_{Lr} + I_L / K \tag{42}$$

If the load current is in a certain range, then the primary current i_p is approximately a constant owing to the large filter inductance. The current i_p and the voltage of the capacitor C_1 and C_2 can be derived as follows:

$$i_p(t) = I_P(t_1) = I_2 , \tag{43}$$

$$v_{C_1}(t) = \frac{I_2}{2C_{lead}}(t - t_1) , \tag{44}$$

$$v_{C_2}(t) = V_{IN} - \frac{I_2}{2C_{lead}}(t - t_1) . \tag{45}$$

However, if the load current continues to decrease, then the primary current cannot be equivalent to a constant current source. The current i_p and the voltage v_{C1} and v_{C2} can be expressed as follows:

$$i_p(t) = I_2 \cos w_2(t - t_1) , \tag{46}$$

$$v_{C_1}(t) = I_2 Z_2 \sin w_2(t - t_2) , \tag{47}$$

$$v_{C_2}(t) = V_{IN} - I_2 Z_2 \sin w_2(t - t_2) , \tag{48}$$

where $Z_2 = \sqrt{(L_r + K^2 \cdot L)/(2C_{lead})}$, $w_2 = 1/\sqrt{2L_r C_{lead}}$.

To ensure ZVS of the leading leg, the leading auxiliary leg should be turned on at a light load level. After adding the leading auxiliary current source I_b, Eqs. (46)–(48) can be derived as

$$i_p(t) = (I_2 + I_b)\cos w_2(t - t_1) - I_b , \tag{49}$$

$$v_{C_1}(t) = (I_2 + I_b) Z_2 \sin w_2(t - t_2) , \tag{50}$$

$$v_{C_2}(t) = V_{IN} - (I_2 + I_b) Z_2 \sin w_2(t - t_2) . \tag{51}$$

In accordance with Eqs. (49) and (50), the ZVS conditions of the leading leg can be summarized either as follows: 1) when the voltage v_{C1} is increased to V_{IN}, the primary current i_p has not decreased to zero; 2) when the current i_p is increased to zero, the auxiliary current I_b provides the remaining energy. Therefore, at the end of mode 3, i_p, v_{c2}, and I_a need to meet the conditions in the following equations:

$$i_p(t) = (I_2 + I_b)\cos w_2(t - t_1) - I_b \ge 0 , \tag{52}$$

$$v_{C_2}(t) = V_{IN} - (I_2 + I_b) Z_2 \sin w_2(t - t_1) \le 0 , \tag{53}$$

$$i_b(t) \ge 0 . \tag{54}$$

In accordance with Eq. (52), the time t_1' when the current i_p drops to zero can be expressed as Eq. (55).

$$t_1' = t_1 + \frac{1}{w_2}\arccos\left(\frac{I_b}{I_b + I_2}\right) \tag{55}$$

At t_1', the voltage v_{C1} can be obtained as

$$\begin{aligned} v_{C_1}(t_1') &= (I_2 + I_b) Z_2 \sin w_2(t_1' - t_1) \\ &= (I_2 + I_b) Z_2 \sin\left[\arccos\left(\frac{I_b}{I_b + I_2}\right)\right] . \end{aligned} \tag{56}$$

If t_1' is taken as the demarcation point, then i_p and v_{C1} can be expressed as follows:

$$\begin{cases} i_p(t) = (I_2 + I_b)\cos w_2(t - t_1) - I_b \\ v_{C_1}(t) = (I_2 + I_b) Z_2 \sin w_2(t - t_1) \end{cases} \quad t \in [t_1, t_1'] \tag{57}$$

$$\begin{cases} i_p(t) = 0 \\ v_{C_1}(t) = v_{C_1}(t_1') + \frac{I_b - I_2}{2C_{lead}}(t - t_1') \end{cases} \quad t \in [t_1', t_2] \tag{58}$$

According to Eq. (57), if i_p is not decreased to zero and v_{C1} is increased to V_{IN}, then v_{C1} needs to meet the conditions in the following equation to ensure ZVS of the leading switches:

$$v_{C_1}(t) = (I_2 + I_b) Z_2 \sin w_2(t - t_1) \ge V_{IN} . \tag{59}$$

Given that $|\sin w_2(t - t_1)| \le 1$, the inequality in Eq. (59) can be derived as

$$(I_2 + I_b) Z_2 \ge V_{IN} . \tag{60}$$

The relationship between I_b and I_L can be expressed as

$$I_b = \frac{V_{IN}}{Z_2} - \frac{I_L}{K} . \tag{61}$$

If I_b=0, then

$$I_L = \frac{KV_{IN}}{Z_2} . \tag{62}$$

According to Eq. (58), if i_p is decreased to zero and v_{C1} is not increased to V_{IN}, then v_{C1} needs to meet the conditions in Eq. (63) to ensure ZVS of the leading switches.

$$v_{C_1}(t) = v_{C_1}(t_1') + \frac{I_b - I_2}{2C_{lead}}(t - t_1') \ge V_{IN} \tag{63}$$

According to Eqs. (56) and (63), the inequality in Eq. (63) is a nonlinear equation. It can be simplified as follows:

$$\frac{I_b - I_2}{2C_{lead}} t_{d(lead)} \ge V_{IN} , \tag{64}$$

where $t_{d(lead)}$ is the dead time of the driving signal for the leading leg.

The relationship between I_b and I_L can be expressed as

$$I_b = \frac{2V_{IN}C_{lead}}{t_{d(lead)}} + \frac{I_L}{K} . \tag{65}$$

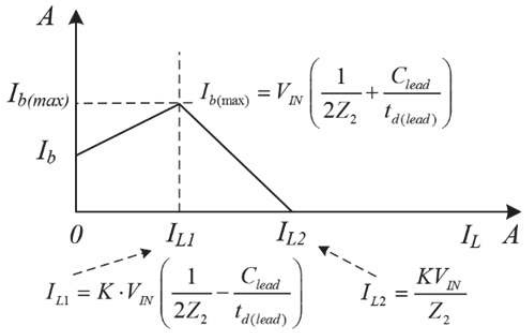

Fig. 9. Curves of i_b and i_L.

In accordance with Eqs. (61) and (65), the maximum value of the leading auxiliary current $I_{b(max)}$ can be derived as

$$I_{\mathrm{b(max)}} = V_{IN}\left(\frac{1}{2Z_2}+\frac{C_{lead}}{t_{d(lead)}}\right). \tag{66}$$

The relationship between I_b and I_L can be expressed as Eq. (67).

$$I_b = \begin{cases} \dfrac{2V_{IN}C_{lead}}{t_{d(lead)}}+\dfrac{I_L}{K} & 0 < I_L \le K \cdot V_{IN}\left(\dfrac{1}{2Z_2}-\dfrac{C_{lead}}{t_{d(lead)}}\right) \\ \dfrac{V_{IN}}{Z_2}-\dfrac{I_L}{K} & K \cdot V_{IN}\left(\dfrac{1}{2Z_2}-\dfrac{C_{lead}}{t_{d(lead)}}\right) < I_L \le \dfrac{KV_{IN}}{Z_2} \\ 0 & I_L > \dfrac{KV_{IN}}{Z_2} \end{cases} \tag{67}$$

In accordance with Eq. (67), Fig. 9 provides the relationship between the leading auxiliary current (i_b) and the load current (i_L).

V. Simulation and Experiment

On the basis of the analysis of the proposed converter, a 50 kW principle prototype of the MTEM transmitter is developed as shown in Fig. 16. The parameters of the MTEM transmitter are shown in Table I.

A. Relationship between the Auxiliary Leg and the Load current

According to Eqs. (40) and (41), when the load current is decreased to 7.05 A, the lagging auxiliary leg needs to be turned on. The maximum current of the resonant inductor L_{r2} can be obtained when the load current is at 3.93 A.

$$I_{a(\max)} = V_{IN}\left(\frac{1}{2Z_1}+\frac{C_{lag}}{t_{d(lag)}}\right) = 3.39A$$

According to Eqs. (66) and (67), when the load current is decreased to 3.01 A, the leading auxiliary leg needs to be turned on. The maximum current of the resonant inductor L_{r1} can be obtained when the load current is at 1.05 A.

$$I_{b(\max)} = V_{IN}\left(\frac{1}{2Z_2}+\frac{C_{lead}}{t_{d(lead)}}\right) = 0.92A$$

TABLE I
Parameters of the MTEM Transmitter

Parameters	Value	Unit
Input voltage	540	V
Resonant inductance	15	μH
Switching frequency	20000	Hz
Output filter inductor	400	μH
Output filter capacitor	990	μF
Resonant capacitor of the leading leg	1	nF
Resonant capacitor of the lagging leg	1	nF
Output voltage	1000	V
Dead time	2	μS
Output current	50	A

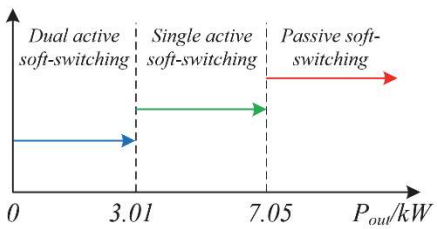

Fig. 10. Relationship between the operating modes and the load power.

In geological explorations, the load of the converter varies with the output frequency. The load impedance may vary from a few ohms to hundreds of ohms with the frequency ranging from low to high. The converter needs to maintain the maximum power output regardless of how the load changes and thus enhance the detection depth and accuracy.

The output voltage and current may not simultaneously reach the rated value in a practical application. At low frequency, the output current reaches 50 A whereas the voltage may not reach 1000 V. At high frequency, the output voltage reaches 1000 V whereas the current may not reach 50 A. Therefore, the relationship between the operating mode and the load current as shown in Fig. 7 can be converted to the relationship between the operating mode and the load power as shown in Fig. 10. The output voltage is 1000 V as shown in Fig. 7, while the voltage is variable as shown in Fig. 10.

B. Determination of the Inductance in the Auxiliary Circuits

In accordance with the waveforms of the auxiliary switches shown in Fig. 5 and the analysis of mode 6 shown in Fig. 6(f), the current of the resonant inductor in the auxiliary circuits can be derived as Eq. (68):

$$I_{\mathrm{aux}} = \frac{V_{IN}T_S}{4L_{aux}} \cdot D_{aux}, \tag{68}$$

where D_{aux} is the duty cycle of the auxiliary legs and T_s is the switching cycle of the auxiliary legs.

According to Eq. (68), the resonant inductance of the leading

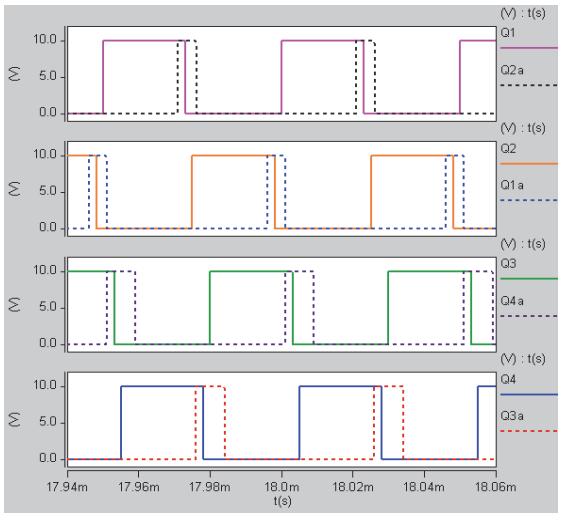

Fig. 11. Driving signals of the main switches and auxiliary switches.

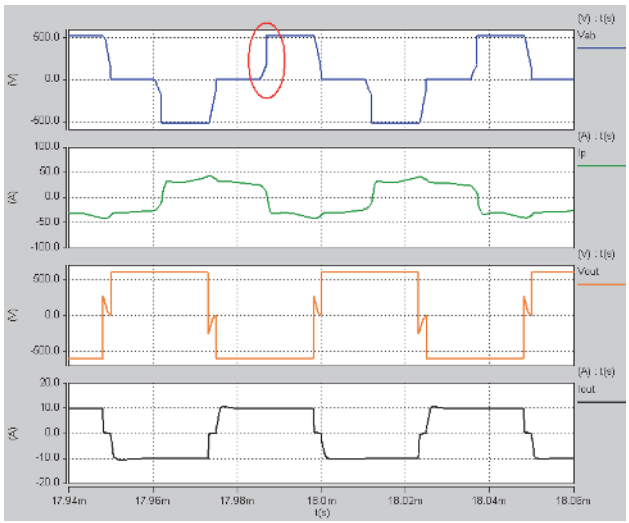

Fig. 12. Main waveforms of the proposed converter in the passive soft-switching mode.

auxiliary leg is equal to 58.9 μH and the resonant inductance of the lagging auxiliary leg is equal to 39.8 μH.

C. Determination of the Auxiliary Winding Ratio

In the design, the falling-edge time of the voltage v_{AB} is generally taken as 5% of the total opening time to reduce the loss and ensure that the main switches achieve ZVS. This condition can be obtained as Eq. (69).

$$T_{falling} = 5\% \cdot T_{on_{\max}} \tag{69}$$

The auxiliary windings ratio is 0.45 according to Eqs. (13) and (69).

D. Simulation Results

On the basis of the said analysis, the dual-active soft-switching converter is simulated with a Saber simulation.

As shown in Fig. 11, the driving waveforms of the main switches and auxiliary switches are consistent with the waveforms shown in Fig. 5.

As shown in Fig. 12, V_{ab} is the voltage waveform between A and B in Fig. 4 and i_p is the current waveform of the primary side. V_{out} represents the output voltage and I_{out} is the output current.

In Fig. 12, the output voltage is 590 V, the output current is 10 A, and the output frequency is 20 kHz. When the output power is 5.9 kW, the lagging switches cannot achieve ZVS as shown in the red cycle of V_{ab}.

As shown in Fig. 13, V_{Q4a} is the drain-to-source voltage of the auxiliary switch Q_{4a} and I_{Lr2} is the current of the resonant inductor L_{r2}. The maximum current value of I_{Lr2} reaches 3.50 A. According to the waveforms of V_{Q4a} and I_{Lr2}, the lagging auxiliary switches achieve zero current switching. Comparing the voltage of V_{ab} in Figs. 12 and 13 shows that the lagging switches achieve ZVS after opening the lagging auxiliary switches.

In Fig. 14, the output voltage is 590 V and the output current

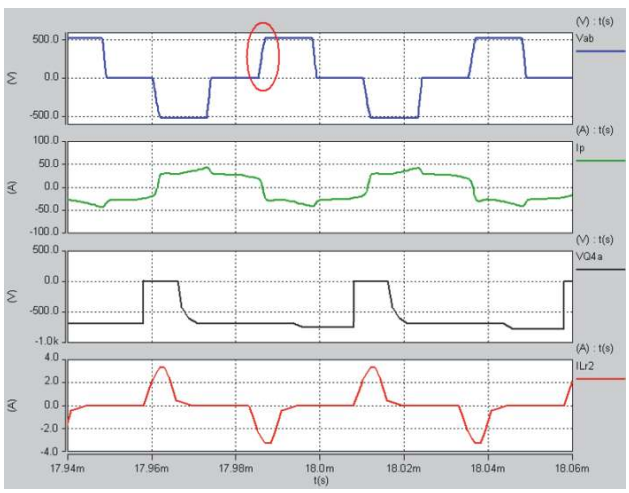

Fig. 13. Main waveforms of the proposed converter in the single-active soft-switching mode.

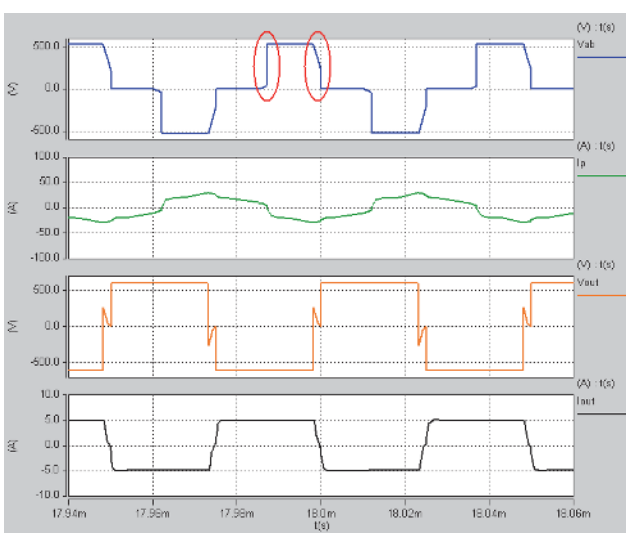

Fig. 14. Main waveforms of the proposed converter in the passive soft-switching mode.

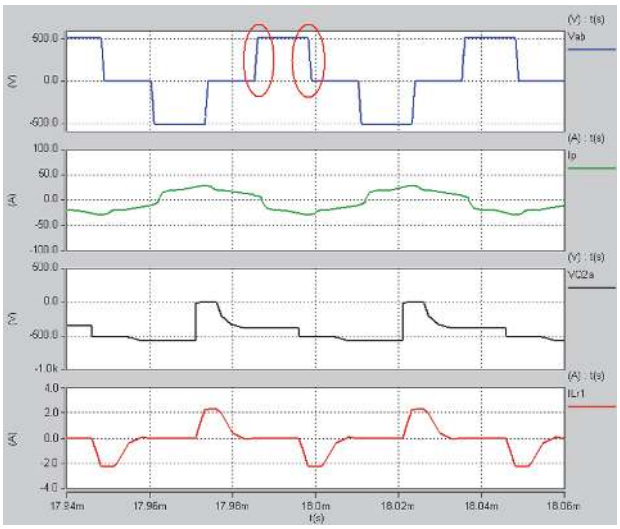

Fig. 15. Main waveforms of the proposed converter in the dual-active soft-switching mode.

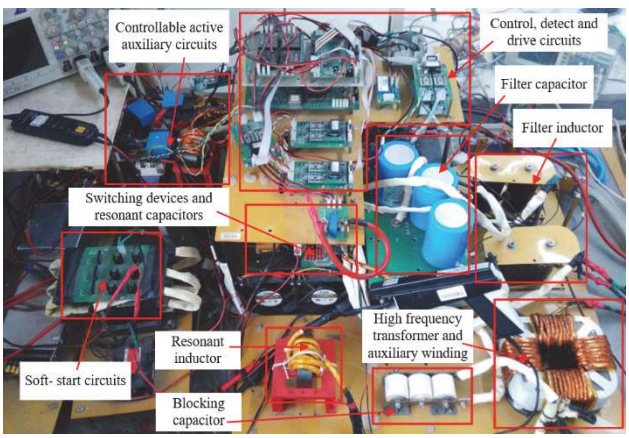

Fig. 16. Prototype of the dual-active soft-switching converter.

is 5.0 A. When the output power is 2.95 kW, the leading and lagging switches cannot achieve ZVS as shown in the red cycle of V_{ab}.

As shown in Fig. 15, V_{Q2a} is the drain-to-source voltage of the auxiliary switch Q_{2a} and I_{Lr1} is the current of the resonant inductor L_{r1}. The maximum current value of I_{Lr1} reaches 2.01 A. Comparing the voltage of V_{ab} in Figs. 14 and 15 shows that the main switches achieve ZVS after opening the leading and lagging auxiliary switches.

E. Experimental Results

On the basis of the aforementioned theoretical analysis and Saber simulation results, a prototype of the dual-active soft-switching converter is implemented as shown in Fig. 16.

The waveforms of the main switches V_{Q1}, V_{Q4} and the auxiliary switches V_{Q2a}, V_{Q3a} are shown in Fig. 17.

As shown in Fig. 18, the light blue waveform (V_{AB}) is the voltage between A and B in Fig. 4 and the purple waveform (i_p) is the current of the primary side. The dark blue waveform (V_{out}) represents the output voltage, the green waveform (I_{out}) is the output current, and the output

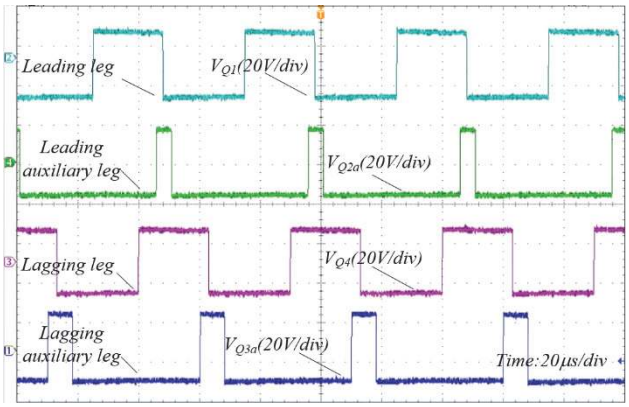

Fig. 17. Driving waveforms of the main switches and the auxiliary switches.

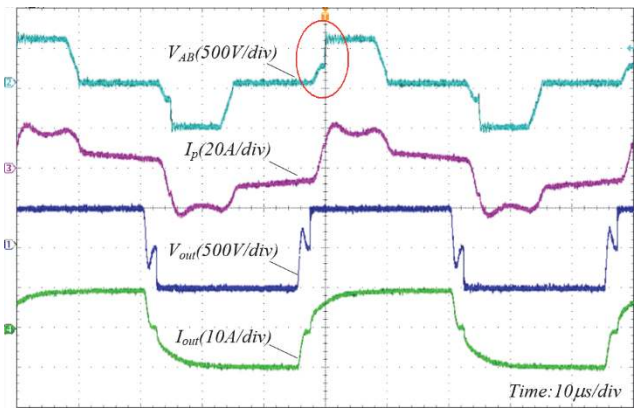

Fig. 18. Main waveforms of the proposed converter in the passive soft-switching mode.

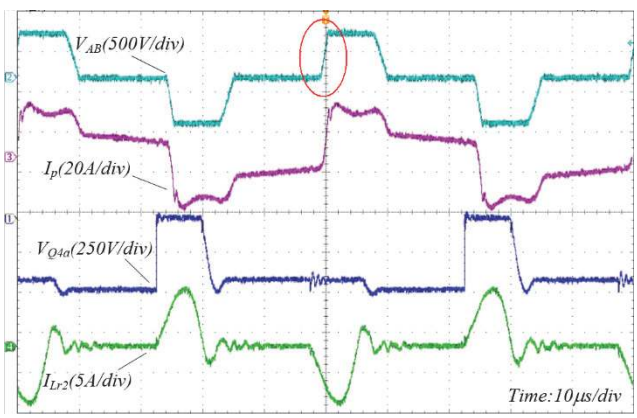

Fig. 19. Main waveforms of the proposed converter in the single-active soft-switching mode.

frequency is 20 kHz.

In Fig. 18, the output voltage is 500 V and the output current is 10 A. When the output power is 5.0 kW, the lagging switches cannot achieve ZVS as shown in the red cycle of V_{AB}.

As shown in Fig. 19, the dark blue waveform (V_{Q4a}) is the drain-to-source voltage of the auxiliary switch Q_{4a} and the green waveform (I_{Lr2}) is the current of the resonant inductor L_{r2}. The maximum current value of I_{Lr2} reaches 7 A. According to

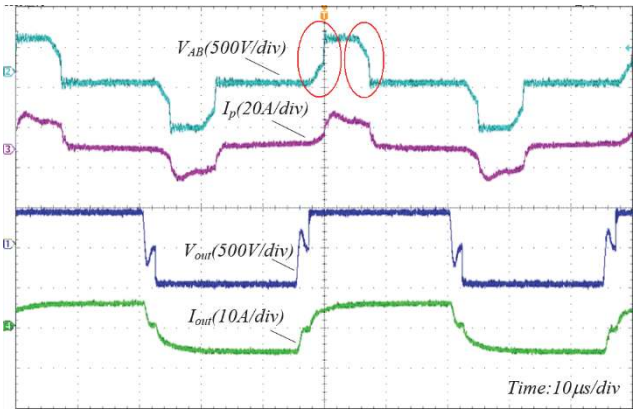

Fig. 20. Main waveforms of the proposed converter in the passive soft-switching mode.

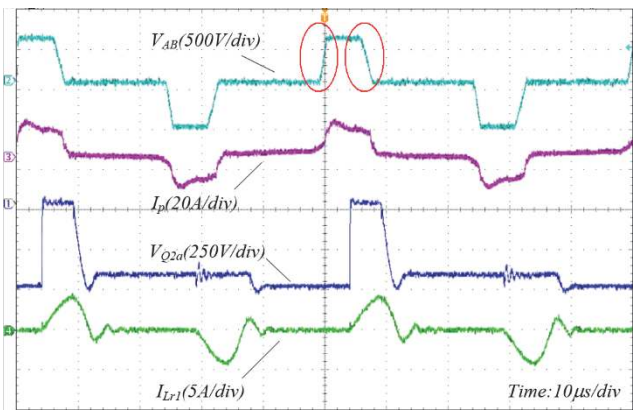

Fig. 21. Main waveforms of the proposed converter in the dual-active soft-switching mode.

the waveforms of V_{Q4a} and I_{Lr2}, the lagging auxiliary switches achieve zero current switching. The switching and conduction losses of the lagging auxiliary switches are greatly reduced. Comparing the voltages of V_{AB} in Figs. 18 and 19 shows that the lagging switches achieve ZVS after opening the lagging auxiliary switches.

In Fig. 20, the output voltage is 480 V and the output current is 6.0 A. When the output power is 2.88 kW, the leading switches and the lagging switches cannot achieve ZVS as shown in the red cycle of V_{AB}.

In Fig. 21, the dark blue waveform (V_{Q2a}) is the drain-to-source voltage of the auxiliary switch Q_{2a} and the green waveform (I_{Lr1}) is the current of the resonant inductor L_{r1}. The maximum current value of I_{Lr1} reaches 4 A. Comparing the voltages of V_{AB} in Figs. 20 and 21 indicates that the main switches achieve ZVS after opening the leading and lagging auxiliary switches.

F. Comparison of the Efficiency

As shown in Fig. 22, the maximum efficiency and power of the traditional transmitter using the hard-switching technology reach 83.7% and 44.5 kW, respectively, while the maximum efficiency and power of the dual-active soft-switching

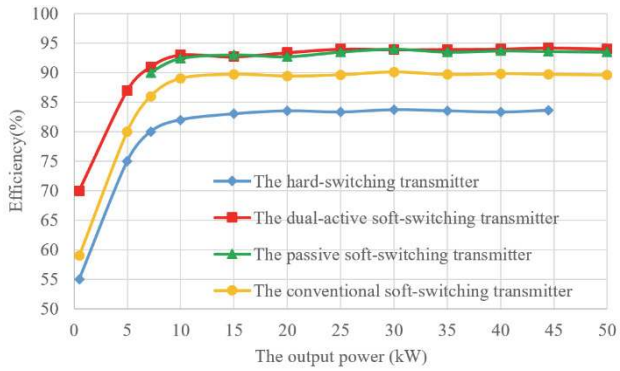

Fig. 22. Measured efficiency of the proposed transmitter and the conventional transmitter.

transmitter reach 94.2% and 50 kW. The maximum efficiency of the conventional soft-switching transmitter reaches 90.1%. Compared with those of the hard-switching transmitter, the efficiency and output power of the proposed transmitter are improved. Unlike that of the conventional soft-switching transmitter, the efficiency of the proposed transmitter is improved. Compared with the passive soft-switching transmitter, the dual-active soft-switching transmitter can achieve ZVS over the entire load range.

VI. CONCLUSIONS

In this study, a novel dual-active soft-switching converter for the MTEM electromagnetic transmitter in the field of geological exploration is proposed. Compared with those of the traditional transmitter, the efficiency and power density per unit volume of the proposed transmitter are greatly improved.

First, the topology of the dual-active soft-switching converter is introduced. Second, combined with the main timing diagram in Fig. 5, the 18 operating modes of the converter are analyzed in detail. Third, three types of operating modes of the proposed converter are presented, namely, the passive soft-switching, single-active soft-switching, and dual-active soft-switching modes. The relationship between the three operating modes and the load power is derived. Meanwhile, the design processes of the leading and lagging auxiliary circuits are presented. Finally, a Saber simulation is carried out for the improved transmitter and a 50 kW principle prototype is proposed. The theoretical analysis, the simulation results, and the experimental results are consistent and verify the correctness and validity of the proposed converter.

The dual-active soft-switching converter ensures the safe and stable operation of the MTEM transmitter under any load conditions.

ACKNOWLEDGMENT

This work was supported by R&D of Instruments and Technologies for Deep Resources Prospecting (the National R&D Projects for Key Scientific Instruments) under Grant No. ZDYZ2012-1-05.

REFERENCES

[1] M. S. Zhdanov, *Geophysical Electromagnetic Theory and Methods*, 1th ed., Netherlands: Elsevier Science, Chap. 4, pp. 135-150, 2009.

[2] A. Ziolkowski, R. Carson, and D. Wright, "New technology to acquire, process, and interpret transient EM data," in *EGM 2007 International Workshop*, pp. 356-359, 2007.

[3] B. Hobbs, A. Ziolkowski, and D. Wright, "Multi-transient electromagnetics (MTEM)–controlled source equipment for subsurface resistivity investigation," in *18th IAGA WG*, Vol. 1, pp. 17-23, 2006.

[4] L. Walker, "MTEM: The next step in EM surveying," in *2-th International Conference & Exposition on Petroleum Geophysics 'Kolkata 2006'*. pp. 5569-1169, 2012.

[5] K. Xue, F. Zhou, S. Wang, and J. Lin, "Constant-current control method of multi-function electromagnetic transmitter," *Review of Scientific Instruments*, Vol. 86, No. 2, pp. 24501-24510, Jun. 2015.

[6] Y. Zhang and P. C. Sen, "A new soft-switching technique for buck, boost, and buck-boost converters," *IEEE Trans. Ind. Appl*., Vol. 39, No. 6, pp. 1775-1782, Nov. 2003.

[7] S. K. Muppidi, C. Anandita, and S. Maddala, *Design & Implementation of Soft-Switching Boost Converter*, 1th ed., LAP LAMBERT Academic Publishing, Chap. 3, pp. 114-128, 2012.

[8] M. Pastor, J. Dudrik, and O. Revak, "High-frequency soft-switching DC-DC converter with full-bridge output rectifier," *Power Electronics and Motion Control Conference (PEMC), 2016 IEEE International*. pp. 110-115, Sep. 2016.

[9] X. B. Ruan, *Soft-Switching PWM Full-Bridge Converters: Topologies, Control, and Design*, 1th ed., John Wiley & Sons, Chap. 3, pp. 52-80, 2014.

[10] S.Y. Lin and C. L. Chen, "Analysis and design for RCD clamped snubber used in output rectifier of phase-shift full-bridge ZVS converters," *IEEE Trans. Ind. Electron.*, Vol. 45, No. 2, pp. 358-359, Apr. 1998.

[11] G. Moschopoulos and P. Jain, "ZVS PWM full-bridge converters with dual auxiliary circuits," in *Conf. INTELEC 2000*, pp. 574-581, 2000.

[12] Z.J. Shen, Y. Xiong, X. Cheng, Y. Fu, and P. Kumar, "Power MOSFET switching loss analysis: A new insight," in *Proc. Industry Applications Conference 2006.* Vol. 3, pp. 1438-1442, 2006.

[13] G. R. Zhu, D. H. Zhang, W. Chen, and F. Luo, "Modeling and analysis of a rectifier voltage stress mechanism in PSFB converter," in *Conf. APEC 2012*, pp. 857-862, 2012.

[14] A. F. Bakan, N. Altintas, and I. Aksoy, "An improved PSFB PWM DC–DC converter for high-power and frequency applications," *IEEE Trans. Power Electron*., Vol. 28, No. 1, pp. 64-74, Apr. 2013.

[15] M. Ordonez and J. E. Quaicoe, "Soft-switching techniques for efficiency gains in full-bridge fuel cell power conversion," *IEEE Trans. Power Electron.*, Vol. 26, No. 2, pp. 482-492, Jul. 2011.

[16] G. Hua, F. C. Lee, and M. M. Jovanovic, "An improved zero-voltage-switched PWM converter using a saturable inductor," in *Conf. Power Electronics Specialists Conference 1991*, pp. 189-194, 1991.

[17] J. A. Sabate, V. Vlatkovic, and R. B. Ridley, "Design considerations for high-voltage high-power full-bridge zero-voltage-switched PWM converter," in *Conf. IEEE APEC 1990*, pp. 275-284, 1990.

[18] J. G. Cho, J. A. Sabate, and F. C. Lee, "Novel full bridge zero-voltage-transition PWM DC/DC converter for high power applications," in *Proc. Applied Power Electronics Conference and Exposition 1994*, pp. 143-149, 1994.

[19] X. Zhang, W. Chen, X. Ruan, and K. Yao, "A novel ZVS PWM phase-shifted full-bridge converter with controlled auxiliary circuit," in *Conf. APEC 2009*, pp. 1067-1072, 2009.

[20] M. Borage, S. Tiwari, and S. Kotaiah, "A passive auxiliary circuit achieves zero-voltage-switching in full-bridge converter over entire conversion range," *IEEE Power Electron. Lett.*, Vol.3, No.4, pp. 141-143, Dec. 2005.

[21] A. J. Mason, D. J. Tschirhart, and P. K. Jain, "New ZVS phase shift modulated full-bridge converter topologies with adaptive energy storage for SOFC application," *IEEE Trans. Power Electron.*, Vol. 23, No. 1, pp. 332-342, Jan. 2008.

[22] G. N. Brahmendra and N. L. Narasamma, "A new active soft-switching circuit for full bridge converters," in *Conf. PEDES* 2012, pp. 1-6, 2012.

[23] A. Sarnowska and J. Rabkowski, "Hard and soft switching operation of the half-bridge based on 900V SiC MOSFETs," in *Conf. IECON 2016*, pp. 7167-7172, 2016.

[24] T. Sun, X. Zhu, H. Liu, L. Liang, and P. Gao, "A novel ZVS PWM FB DC/DC converter using auxiliary resonant net," in *Power Electronics and Motion Control Conference 2006*, pp. 728-732, 2006.

[25] Y. Jang and M. M. Jovanovic, "A new family of full-bridge ZVS converters," in *Applied Power Electronics Conference and Exposition,* Vol. 2, pp. 622-628, 2003.

[26] M. Borage, S. Tiwari, S. Bhardwaj, and S. Kotaiah, "A full-bridge DC–DC converter with zero-voltage-switching over the entire conversion range," *IEEE Trans. Power Electron.*, Vol. 23, No. 4, pp. 1743-1750, Jul. 2008.

Xuhong Wang was born in Hebei, China, in 1987. He received his B.E. from the School of Electrical and Electronic Engineering, Shijiazhuang Tie Dao University, Hebei, China, in 2011, and he received his M.E. from the Faculty of Information Technology, Beijing University of Technology, Beijing, China in 2014. He is currently working toward his Ph.D. in the Faculty of Information Technology, Beijing University of Technology, Beijing, China. He is participating in research on quality control of electrical equipment, electric tests, and tests on the electromagnetic compatibility of electrical and electronic equipment. His current research interests include modeling, control, simulation and design of switching power supplies, and system optimization concerning electromagnetic fields and high voltages.

Yiming Zhang was born in Hubei, China, in 1964. He received his B.E. from the School of Electronic, Information and Electrical Engineering, Shanghai Jiao Tong University, Shanghai, China, in 1988, and his M.E. from the School of Electrical Engineering and Automation, Harbin Institute of Technology, Harbin, China in 1992. From 2000 to 2007, he was a Senior Researcher in the Institute of Electrical Engineering, Chinese Academy of Sciences, Beijing, China. Since 2008, he has been a Professor in the College of Electronic Information and Control Engineering, Beijing University of

Technology, Beijing, China. His current research interests include intelligent power management, motor speed control, servo drivers, and motor energy conservation.

Wei Liu was born in Hubei, China, in 1993. He received his B.E. from the School of Automobile and Mechanical Engineering, Changsha University of Science & Technology, Hunan, China, in 2015. He is currently working toward his M.E. in the Faculty of Information Technology, Beijing University of Technology, Beijing, China. He is participating in the research on quality control of electrical equipment and reducing the power loss of electronic device. His current research interests include analyses of power quality for electric system in some professional fields, control and design of switching power supplies, and system optimization concerning electromagnetic fields.